Reactor pressure vessel embrittlement: Insights from neural network modelling

Mathew, J, Parfitt, D, Wilford, K, Riddle, N, Alamaniotis, M, Chroneos, A & Fitzpatrick, ME

Original citation & hyperlink:
Mathew, J, Parfitt, D, Wilford, K, Riddle, N, Alamaniotis, M, Chroneos, A & Fitzpatrick, ME 2018, 'Reactor pressure vessel embrittlement: Insights from neural network modelling' *Journal of Nuclear Materials*, vol 502, pp. 311-322
https://dx.doi.org/10.1016/j.jnucmat.2018.02.027

DOI 10.1016/j.jnucmat.2018.02.027
ISSN 0022-3115

Publisher: Elsevier

Reactor Pressure Vessel Embrittlement: Insights from Neural Network Modelling

J. Mathew[1(a)], D. Parfitt[1], K. Wilford[2], N. Riddle[2], M. Alamaniotis[3], A. Chroneos[1], M.E. Fitzpatrick[1]

[1]Faculty of Engineering, Environment and Computing, Coventry University, Priory Street, Coventry CV1 5FB, United Kingdom

[2]Materials, Chemistry and Corrosion, Rolls-Royce plc, PO Box 2000, Derby, DE21 7XX

[3]School of Nuclear Engineering, Purdue University, West Lafayette, IN 47907, USA

Abstract

Irradiation embrittlement of steel pressure vessels is an important consideration for the operation of current and future light water nuclear reactors. In this study we employ an ensemble of artificial neural networks in order to provide predictions of the embrittlement using two literature datasets, one based on US surveillance data and the second from the IVAR experiment. We use these networks to examine trends with input variables and to assess various literature models including compositional effects and the role of flux and temperature. Overall, the networks agree with the existing literature models and we comment on their more general use in predicting irradiation embrittlement.

Keywords: Reactor Pressure Vessel Embrittlement, Irradiation Damage, Neural Networks.

[a)]Electronic mail: jino.mathew@coventry.ac.uk

1 Introduction

The reactor pressure vessels of most modern light-water reactors are constructed from low alloy ferritic steel forgings and welds, as these offer a combination of high strength, high toughness and ease of fabrication in large sections [1]. These steels, however, suffer from irradiation embrittlement, where damage from neutrons from the reactor core causes the formation of many atomic-scale defects within the metal grains [2]. These defects impede the motion of dislocations, leading to an increase in the hardness and a reduction in ductility of the steel. During its lifetime the vessel therefore becomes progressively more susceptible to brittle failure. The failure of a reactor pressure vessel is unacceptable, and as the vessels are not replaceable, predicting the embrittlement of these steels is fundamental in ensuring the safe, continued operation of nuclear reactors. In severe cases, the embrittlement of the vessel may erode the safety margins against brittle failure to such an extent that it is no longer permissible to operate the reactor.

A large quantity of data has been accumulated by the international community on irradiation-embrittled steels: in particular many international codes (including the US, French and Japanese industries [3–5]) mandate the use of pressure vessel surveillance samples that, once withdrawn and tested, provide an estimate of the likely embrittlement over time [4]. These data have been collated into several international datasets [6] and are supported by extensive test reactor programmes [7] which have seen steel samples irradiated under vastly accelerated test conditions in order to provide a wider range of compositions, test methods [8] and microstructural characterisation [9] than would be possible from the limited, multi-year surveillance data.

In addition to the experimental programme, significant efforts have been made in order to develop a better understanding of these phenomena. These have approached the problem by incorporating physical understanding into existing models [10, 11], by developing a model on

sound reasoning and fitting the resulting parameters to data [12, 13], or by developing a model using solely modelling and simulation [14]. The preference for physical understanding over empiricism is fundamental in reducing risk and is reflected in the considerable research undertaken by the industry.

Despite the significant improvements in physical modelling, there are still gaps in the understanding of irradiation damage in these steels which will persist for many years. For example, there is a current debate over the importance of Ni/Mn/Si precipitates which may form late-on in the lifetime of a reactor [15]; also, there is no universal agreement on how to use short-term surveillance datasets, obtained over only a few years, to the 40 or 60 year design lifetime of modern reactor vessels.

The greatest challenge, however, is to identify a correlation between the various exposure parameters, of which there are many. One of the most important variables is irradiation temperature, and data have been collected on embrittlement in steels at many temperatures. However, taking these data and predicting the actual temperature-dependence of embrittlement in a particular steel is a non-trivial exercise because of the number of other input variables; and more seriously, that the temperature effect itself may vary with both the irradiation flux [16] and the composition of the steel (specifically there is substantial interest to investigate the dependence on Ni-content [17]). These problems are compounded by the high cost and long timescale of irradiated materials testing.

Artificial neural networks (ANNs) [18] are powerful computational models based on empirical regression that can be used to learn dependencies or patterns existing in data. ANNs are generally constituted by layers of interconnected processing elements called neurons that replicate the functionality of a biological neuron. In training, the network coefficients, described as weights and biases, are optimised based on minimisation of an error function such as a ‘mean squared error’. A back-propagation algorithm [19] is commonly used for training,

which mostly relies on gradient descent techniques for optimisation of weights. A typical architecture for a neural network comprises a two layer perceptron where the input nodes are connected to the so-called "hidden layer" which is subsequently connected to the output. The input/output mapping is processed in each of the hidden neurons using the non-linear activation function.

Previous work has shown the use of ANN to account for various measures of irradiation damage. For example they have been used to predict hardening and Charpy transition temperature shifts in irradiated steels [20, 21] at high values of fluence in support of the development of low activation steels. More recently, Castin and co-workers [22] have used ANNs to predict irradiation induced change in yield stress and examine the relative importance of different irradiation variables. This study shows the ability of the networks to make complex, subtle predictions of irradiation induced change from a relatively small database of irradiation damage results.

In this study, we intend to improve the understanding of the role of critical input parameters such as flux, fluence, temperature and chemical composition on the irradiation-induced ductile-to-brittle transition temperature shifts. Specifically we develop the ANNs to assess the effect of a single variable upon the embrittlement in the absence of any prior assumptions as to the functional form and compare the predictions with established physical models. We also use these models to examine the likely effects (or absence of effects) of irradiation parameters such as flux and temperature.

This paper is organised as follows. In the method section we explain the form and structure of the artificial neural network and discuss the dataset used in the model, including the partitioning into the training and test datasets. In the results section, we show that the model is comparable with several current embrittlement trend curves; we also show estimates of the shift change in response to several input variables in order to provide support to several

different physical models. In the discussion section, we provide a perspective on the use of these models to comment on several important current themes in irradiation damage and to provide a framework for the development of physically based models.

2 Method

2.1 Databases

There is a wide range of data available in the international literature on pressure vessel steel embrittlement. For this paper we consider two separate datasets. The first is the IVAR data [23] from the Irradiation Variables Experiment led by Odette and co-workers. This is a dataset that looked at a wide range of different steel compositions under extremely well-controlled temperature, flux and fluence conditions; however these data were collected in test reactor conditions using a significantly higher fast neutron flux than a normal pressurised water reactor vessel may experience. We have selected the CM-series alloys from these datasets as despite being split melt model steels the compositions bracketed those of traditional pressure vessel steels; the variable-stress-relief steels or more exotic compositions were not included. This restriction gave a total of 756 data within this set. The second dataset we consider comes from the US civil power database (NUREG) [6] and contains the accumulated experience from irradiated surveillance samples from US operators.

The range of the database in terms of flux and fluence is shown in Figure 1. It is evident that although the datasets reach similar fluence values, the IVAR data is on average at higher flux than the NUREG data. For comparison, in this figure, two lines illustrate an approximate end of life fluence for a nuclear pressure vessel operating for 60 years, and the typical surveillance data assuming a lead-factor equal to four i.e. the ratio of neutron fluence rate at the capsule to the rate at the vessel inside surface. Data from the IVAR experiment are

measured in terms of change in proof strength. For ease of comparison between the two datasets and with other literature values, we have converted the measured values of proof strength into an effective shift in Charpy transition temperature, as measured in the NUREG database; the conversion factor used is 0.6°C/MPa.

Temperature is an important variable determining the level of irradiation embrittlement of a material. All of the NUREG data have been collected at typical reactor operating temperatures between 275°C and 290°C; the IVAR data uses irradiations at three different temperatures: 270°C, 290°C and 310°C. In Figure 2 the range of compositions included in the IVAR dataset is also illustrated.

2.2 Artificial Neural Network (ANN) modelling

ANNs are useful to identify highly-complex and non-linear relationships between the output and input data [24]. Prior knowledge on the correlation between the input variables and the output is generally not required to find pertinent solutions using the data. A feed-forward multi-layer perceptron (MLP) architecture [25] with one hidden layer was undertaken using the MATLAB neural network toolbox [26]. This architecture is chosen as it is well understood that MLPs have universal approximation capabilities [27]. A scaled conjugate gradient [28] training regime was implemented using a log-sigmoid transfer function in the hidden layer and linear transfer function in the output layer. The neurons in each layer are inter-connected to the neurons in the succeeding layer through a synaptic weight and bias. The net output z from the ANN can be expressed as,

$$z = \sum_{j=1}^{H} w_j \log h\left[\sum_{i=1}^{8} w_{ji} a_i + b^{(1)}\right] + b^{(2)} \quad (1)$$

where w_j is the weight matrix in output layer, w_{ji} the weight matrix in the hidden layer, $b^{(1)}$ bias vector in the first layer, $b^{(2)}$ bias vector in the second layer, H number of hidden neurons

and a_i the input variables.

Unlike traditional trend curves, ANNs can be used to specify a convoluted mapping pertaining to surveillance data without having any prior assumptions. Nevertheless, susceptibility to overfitting is one of the major drawbacks: i.e. when the network generalises poorly and fits the inherent noise in the data rather than the underlying pattern. The Bayesian approach [29] aims to avoid the phenomena of overfitting through marginalisation of network output by adding penalty terms to the error function thereby eliminating networks with implausibly large weights. The weights are initialised by assuming a Gaussian distribution having the mean centred at zero with one standard deviation. It is often beneficial to initialise weights with small random values to avoid premature saturation of the sigmoidal functions [30].

The number of neurons in the hidden layer controls the complexity of the model, and use of over-complex models is not permissible in the Bayesian technique. It is also vital to have an unseen test dataset to evaluate the generalisation ability of the network: this is also known cross-validation [18]. The test dataset was created by randomly selecting samples from the experimental dataset. In order to optimise the number of hidden units, the network was trained using 5 to 20 and the moving average trendline of root mean square error (RMSE) was determined for the test and training datasets using:

$$RMSE = \sqrt{\frac{\sum_{n=1}^{M} \left(t_n - z_n\right)^2}{M}} \qquad (2)$$

where t is the target value, z the output, M is the number of samples.

The minimum RMSE error was first obtained for the training and test datasets with 11 neurons (see Figure 3). The test error shows the generalisation ability of the neural network whereas the training error is a measure of fitting uncertainty in the data.

A schematic of the network architecture is shown in Figure 4. The flux and fluence

parameters were normalised in the range –1 to +1 primarily because of the magnitude being higher by several orders compared to other input variables, and to fully utilise the capability of the log-sigmoid transfer function. The functional form of fluence and flux parameters were optimised after evaluating the RMSE error during the training (see Table 1). The use of physically motivated parameters such as $(\text{flux})^{1/2}$ and $(\text{fluence})^{1/2}$ was found to reduce the scatter and RMSE error in the resulting ANN predictions. The generalisation ability of the network can also be enhanced by using an ensemble of networks and combining predictions formed from multiple networks [31]. Moreover, the training process is completed when the error function reaches a 'minima' and the danger of getting trapped in a local minimum is very likely. Committee networks initialised to random values of weights can be effectively used to tackle this problem. An ensemble of 250 networks was developed by running independent training sessions and the predictions were marginalised by using the Bayesian error function E_S described in equation (3):

$$E_S = \frac{\beta}{2}\sum^{M}\{t - z(a,w)\}^2 + \frac{\alpha}{2}\sum^{R}\left|w_i\right|^2 \qquad (3)$$

where β is the parameter controlling the variance in noise, α is the regularisation coefficient, w the weight vector, t the target value and z the output. The transition temperature shift is obtained from the mean of the marginalised set of predictions with error bars corresponding to $\pm 1\sigma$ (standard deviation). The large error bars signify regions of sparse training data, lack of degrees of freedom to fit the desired input/output mapping, or the inherent noise existing in the input process parameter space [18].

3 Results

The overall quality of fit of the ANNs to the IVAR and NUREG databases is illustrated in Figure 5, showing both all of the available data and those reserved from the fitting process.

The ANNs overall reproduce the trends in the data, particularly considering the wide range of input variables. For comparison with previous work, we calculate the mean error in the M predictions, e, according to:

$$e = \frac{\sum_{n=1}^{M} |t_n - z_n|}{M}$$

And then bias b:

$$b = \frac{\sum_{n=1}^{M} t_n - z_n}{M}$$

As estimates of the overall performance of the ANNs in reproducing the data. The calculated values converted into change in yield strength (for comparison with Castin and coworkers [22]) and the values are reproduced in Table 2. The IVAR predictions display a similar level of uncertainty to the previous work: The Castin data are fitted to the RADAMO database which, similar to the IVAR database, contains data from a test reactor with controlled values of flux, fluence, temperature and composition [32] and the total error and bias are similar. The NUREG data are more scattered. The uncertainty in the network predictions are a function of both the number of input variables and the distribution of data and therefore the greater scatter in the NUREG predictions are likely due to the lack of homogeneity in the variables from these data.

In the section that follows, we discuss in turn the variation of embrittlement shift as a function of temperature and flux. Following this we discuss the effect of composition upon the magnitude of the shift. In the discussion section, we analyse further these data and compare them to various literature models of embrittlement shift.

3.1 Irradiation Temperature Dependence

The irradiation temperature has a significant effect on the level of embrittlement. Physically this is attributed to the effect of temperature on the balance between defect creation, migration, and annihilation. The NUREG database is based on surveillance data and has a

relatively small temperature range and therefore we exclude it from the analysis in this section. The IVAR database was deliberately targeted at investigating temperature ranges. Figure 6 shows the predicted changes in irradiation embrittlement using a neural network fitted to this dataset. Overall, the level of irradiation embrittlement increases as the temperature decreases showing approximate linear dependence, and this is in good agreement with the current understanding of irradiation damage [33, 34].

Similar linear trends are observed for a wide range of steel compositions, in particular both high and low Cu (Figure 6(a)). In the EONY model, irradiation damage shift is attributed to two features, matrix damage (Cu < 0.072 wt. %) and both matrix damage and Cu-precipitate formation for (Cu > 0.072 wt. %). The data in Figure 6(a) show similar trends with temperature suggesting that the increase in embrittlement at lower temperature arises from a common decrease in solute solubility or an increase in the effectiveness of radiation-induced defects (e.g. vacancies and interstitials) in forming defects, rather than a change in the nature of the embrittlement features. This is based on the assumption that in a high-Cu steel the dominant hardening features are Cu precipitates and in a low-Cu steel they are matrix damage (e.g. interstitial loops formed during the irradiation cascades).

3.2 Flux Dependence

The dependence of irradiation embrittlement on the flux or dose rate is a complex and sometimes controversial topic [16]. It is important because high fluence data is crucial to justifying the long term operation of reactor pressure vessels but this often relies upon accelerated irradiations at high flux in order to generate the required fluences within a feasible timeframe. The argument for flux effects is that interstitial and vacancy pairs in high flux irradiations have increased rates of matrix recombination which results in a shorter average lifetime and therefore a lower overall mobility of solute atoms. This results in high flux irradiation having less total embrittlement due to solute clustering for a given fluence. The

argument is based on sound physical reasoning (for example rate theory modelling of defect survival rates [35]) but whether this provides a significant effect in complex steel irradiations depends upon the temperature of the irradiation, the nature of the embrittling features and the composition of the steel.

In high Cu steels, low fluence irradiations show a flux effect as the decreased vacancy survival lifetimes lead to a delay in the formation of Cu precipitates; in high fluence, high Cu steels there is little or no flux effect as all of the matrix Cu has been incorporated into precipitates and the lower diffusivity has no longer any effect [35]. In low Cu steels, there is a lack of consensus on flux effects which mirrors the lack of certainty as to the importance of solute clustering in their evolution. The EONY model and the analysis of the IVAR database both concluded that flux effects were present (and displayed similar trends) in low-flux surveillance data ($\varphi \sim 1\times10^{8}$-$1\times10^{10}$ n/cm^{2}s^{-1}) and in the IVAR dataset ($\varphi \sim 1\times10^{11}$-$1\times10^{12}$ n/cm^{2}s^{-1}) [12] and other researchers have adopted similar factors [36]. However other researchers have not found supporting evidence for flux or dose rate effects in low Cu steels in their surveillance data or in targeted high flux irradiations on specific materials [37].

The most common method of compensating for a flux effect (if present) is to ascribe an effective fluence:

$$\phi t_e(\phi) = Q(\phi)\phi t_r \qquad (4)$$

Where ϕt_r is an arbitrary reference fluence and $Q(\phi)$ is a scaling factor. The effective fluence can then be used in an embrittlement trend curve that does not vary with flux. Using this method may give significant improvement in the quality of fit of a given trend curve.

To calculate the value of Q as a function of flux we concentrate on low Cu steels and assume that the embrittlement follows a square-root dependence on the fluence, i.e. the

embrittlement follows a trend:

$$\Delta T_{41J} = A(\phi t)^{1/2} \quad (5)$$

Where A is a parameter incorporating the material, flux and temperature sensitivity of the steel. This assumption is consistent to the functional form of fluence used to train the ANN (see Table 1) and, unlike analytical functions, ANN in its present form cannot be used to calculate the fluence required to reach a given shift value.

The effective fluence can be linked to the reference fluence at a reference flux and the square of the ratio of the embrittlement at this reference fluence at the two fluxes:

$$\phi t_e = \phi t_r \left(\frac{\Delta T_{41J}(\phi t_r, \phi_r,)}{\Delta T_{41J}(\phi t_r, \phi)} \right)^2 = Q(\phi)\phi t_r \quad (6)$$

Therefore we can evaluate the approximate acceleration factor $Q(\phi)$ through calculating this ratio as a function of flux.

The NUREG database contains mainly lower flux surveillance data. Analysis of this dataset using the ANNs reveals an effect of flux but not one that is significant given the uncertainty in the predictions. We illustrate the trends for low Cu, low and high Ni steels in Figure 7(a) where it can be seen that the shift drops over the flux range considered but the error bars on the predictions do not support a significant effect. We show in Figure 7(b) the same data converted into an acceleration factor.

The IVAR database has been used to make predictions of irradiation shift at higher flux values between 1×10^{11} and 1×10^{12} n/cm^{2}s^{-1}. These data show more evident flux effects. Figure 8(a) and (b) shows predicted embrittlement shifts for low Cu, high and low Ni steels and a high Cu, high Ni steel. The steels all show a drop in the predicted embrittlement as the flux is increased for a constant fluence, though the drop in the high Cu steel is marginal given the uncertainty in the predictions. Comparing the effective fluence, Figure 8(b), suggests that both the low Cu steels have a significant flux effect associated with their embrittlement, whereas

the high Cu steel has much less of an effect. The data here are plotted for a fluence of 1.1×10^{19} n/cm^2 i.e. a level where we would expect the matrix Cu to be fully depleted, the lack of a significant flux effect is therefore in line with the expectations for these conditions.

The composition of the steel appears to have a relatively minor effect upon the shape of the flux curve, with the notable exception of very low Ni contents. This is illustrated in Figure 8 (a) and (b) where we show there is a significant increase in the effect of flux for the low Ni case (C_{Ni}=0.1 wt. %) compared with high Ni (C_{Ni}=1.5 wt. %). Other compositional trends (Figure 8(c) and (d)) show the example of Mn and P) have much less effect on the shape of the trend curve. It is not clear what the reason for the dependence on Ni is in these steels: it may be attributed to the very low values of shift in steels with low Ni but it should also be noted that there are few very low and very high values of Ni within the IVAR dataset in order to make a systematic comparison.

3.3 Compositional dependence

The compositional dependences of irradiation embrittlement are important to understand because the large number of correlated variables often confound traditional trend curve fitting. In this case, we consider the behaviour of steels with differing levels of Ni, Mn and Cu. These are important variables because they can vary widely between different grades of steel (for example Ni contents within the US database range from 0.3 to 1.6 wt%) and therefore incorrect weighting of these variables can cause significant problems when extrapolated to new compositions. High Ni levels are often associated with increased levels of embrittlement, but also bring benefits of higher un-irradiated strength, better start-of-life toughness and lower levels of segregation during forging. Balancing these differing factors is an important part of the development of new, lower-cost vessel alloys and fabrication routes.

Figure 9 shows the overall dependence of embrittlement shift from the IVAR data as a function of the same compositional variables plotted in Figure 2. This is calculated for a

medium fluence (1×10^{19}n/cm^2), low IVAR flux (1×10^{11}n/cm^{2}s^{-1}), and a temperature of 290°C. There is an unsurprising influence of Cu on the shift, although interestingly there is not a distinct division between 'high' and 'low' Cu steels. The influence of Ni is also significant though this occurs over a much broader range of compositions than any of the other solute species. The role of other species in determining the embrittlement shift is comparatively minor, with Mn in particular not predicted to have a strong effect on the total magnitude of shift despite the relatively large variation in total content. There is also reassuringly little evidence for strong non-linearity between the various different compositional terms, although there is some suggestion of a complicated relationship between Ni and Si.

The compositional trends result in similar conclusions to those of Castin and co-workers in a previous study of ANNs for shift prediction [22]. The lack of strong dependence on Si and Mn mirrors the findings that Cu and Ni were the most significant input variables in determining shift and it was difficult to unpick separate contributions due to other alloying elements. Comparison with linear regression of the IVAR database (for example Table 4.2 of Reference [23]) also supports these conclusions with the relative changes in shift of low Cu steels as ~30°C/wt.% Ni and ~16°C/wt% Mn.

4.0 Discussion

In this discussion section we look at the comparison of the ANN models with literature predictions, and the influence of irradiation variables upon the overall shift. We begin by comparing the ANN shift predictions for a subset of IVAR alloys to those obtained using more established models. For example, Figure 10 shows a selection of embrittlement predictions for the IVAR alloys CM16 and CM17, differing primarily in their Ni contents, with a flux of 7.8×10^{11} n/cm^{2}s^{-1} ('high flux' in the IVAR designations) and temperature of 290°C. This shows the original IVAR data (with similar fluxes selected) but compared with the ANN model

predictions plus error bands of two standard deviations. The ANN model does an acceptable job of predicting the data. We also compared these data with the predictions from the EONY model [12].

The data in Figure 10 demonstrates one of the drawbacks of the ANN approach compared to more physically based modelling. Firstly, the predictions may be associated with rather high uncertainties even for compositions within the database as evidenced by the comparison of CM16 and CM17. Secondly, we can see that outside of the range of the data the uncertainties grow significantly, and the predictions themselves may not follow a realistic trend. We can see in Figure 10 that the curve fails to tend to zero at low values of fluence although zero is within the predicted uncertainty. This is also illustrated in Figure 7, where extrapolation of the NUREG database outside of the flux region where the majority of the data lie comes with an increase in the uncertainty of the predictions.

4.1 Jones and Williams Temperature Model

The most extensive empirical study of the trend in irradiation embrittlement as a function of temperature is that of Jones and Williams [33], based on data initially taken from carbon-manganese steels used in the UK nuclear industry. The Jones and Williams model predicts the irradiation shift in low-Cu steels (less than 0.1 wt% Cu) relative to the shift at a reference temperature T_R. In the original formulation of the model, this was expressed as a change in yield stress of the material, however on the assumption that this will linearly correlate with the change in T_{41J} Charpy reference temperature we write:

$$\Delta T_{41J}(T) = \Delta T_{41J}(T_R) \times \left(\frac{a - bT}{a - bT_R} \right) \tag{7}$$

Where a and b are fitted parameters which are originally reported as 1.869 and 4.57×10^{-3} °C^{-1} and refitted with additional data as 1.848 and 4.58×10^{-3} °C^{-1} [33]. The reference temperature

T_R is arbitrary and is normally quoted as 190°C.

Figure 6 demonstrated that the ANN predictions were approximately linear with temperature, which is in agreement with the Jones and Williams model. Using these data we have investigated any variation in these trends with steel composition. We show in Figure 11 the results of linear fits to the temperature variation for a variety of compositions: for simplicity we take T_R=0°C and compare the ratio b/a in the Jones and Williams model (2.48×10^{-3}) with the numerical gradient of the temperature plots. This demonstrates that overall the predictions are in agreement with the literature model. We can however also examine more subtle variations with different compositions. Si and Mn have little effect upon the gradient; however both Cu and P have an effect. In the case of Cu, this may be due to an additional contribution of Cu precipitation (as well as matrix damage) where at lower temperatures the lower solubility of Cu may lead to greater amounts available for precipitation. This is reinforced by the observation that the effect is more pronounced in the higher rather than the lower fluence data. The role of P is more uncertain, there are no reports of grain boundary embrittlement in the tested steels so it would seem unlikely that this is an effect due to non-hardening embrittlement.

The effect of Ni content on the temperature variation is also worthy of comment. There is a small but significant increase in the temperature sensitivity dropping from a high-Ni (C_{Ni}=1.6 wt.%) steel to a very low Ni (C_{Ni}=1.6 wt.%). This is in line with more complex temperature trends: in particular, Odette et al. [23] and Williams et al. [36] suggest a link between Ni content, C_{Ni}, and the temperature factor. In this case, the most recent formulation is a shift in embrittlement of:

$$\Delta T_{41J}(T) = \left[1-\left(a+bC_{Ni}\right)\left(\frac{1}{T_R}-\frac{1}{T}\right)\right]\Delta T_{41J}(T_R) \qquad (8)$$

Where a=1117, b=180.8 per wt. % and again we have assumed a linear relationship between the shift in 41J Charpy energy and the hardness changes reported in the original reference. The

predicted trends are all close to linear and so it was not possible to distinguish between these linear models and the more complex exponential dependence proposed by Debarberis and co-workers [34].

4.2 Comparison with Flux Models

The variation of embrittlement with irradiation flux at a given fluence determines the embrittlement shift in a real reactor vessel when extrapolated from accelerated surveillance data collected over a third to a fifth of the reactor operating lifetime [4]. It is of great practical importance as current operating nuclear power plants are justified to be safe partly based on these data. The introduction of new materials and methods into the next generation of nuclear power plants also relies upon being able to collect relevant embrittlement data in advance of first operation which will require the use of greatly accelerated test irradiations in order to provide an initial safety justification.

The flux effect has a sound physical basis on precipitation which has been captured through rate-theory modelling of irradiation-induced Frenkel pairs and their subsequent effect on the diffusion of solute species within the steel [38, 39]. Essentially, as flux is increased the rate of vacancy generation increases but the fractions diffusing over long distances to fixed sinks (dislocations or grain boundaries) reduces due to increased recombination in the region local to the cascade [35]. The effect of these vacancies on radiation enhanced diffusion therefore increases with flux, but not as much as would be expected due to the decrease in the average lifetime of a vacancy. The question for the embrittlement of RPV steels is whether this effect is significant (and therefore requires separate accounting) when extrapolating from a high flux value to a realistic RPV wall value. This depends upon the range of flux, the composition of the steel, the fluence reached and the irradiation temperature.

The presupposition of any trend curve linking high and low flux irradiations is also important to test. Very high flux irradiations, either from short test reactor exposure or

(increasingly) from ion-beam implantation are very attractive to the community as they achieve very high doses in a short time, allow a much greater range of material conditions to be assessed; and in the case of ion-beam implantation, do so without generating significant levels of radioactivity in the samples. For these data to be useful, even just as a screening method for new materials or manufacturing processes, the embrittlement must be shown to share the same physical origin as that occurring at reactor pressure vessel wall dose rates, i.e. the dominant contributions should come from solute precipitation or matrix damage. The current uncertainty over the role of high flux features limits the adoption of these potentially valuable techniques and data.

Figure 7 demonstrates evidence of an effect of flux in low Cu steels within the ranges considered in the IVAR dataset and this also shows the reduction in the efficiency of the irradiation to a given fluence in producing damage in the steel. For comparison with literature models of this effect, it is common practice to link the effective fluence to a scaling parameter $p(\phi)$ and the ratio of fluxes:

$$\phi t_e(\phi) = Q(\phi)\phi t_r = \left(\frac{\phi_r}{\phi}\right)^{p(\phi)} .\phi t_r \qquad (9)$$

Where $p(\phi) = 0$ would be the absence of any flux effect. The value of $p(\phi)$ calculated from the ANNs is presented in Figure 12 as a function of flux. Literature values of $p(\phi)$ (which are often averaged over a range of fluxes) are normally in the range 0.15-0.25 and we also note the close coincidence of the values and trends of these curves with the analytical expressions given in the work [12, 35]. The EONY model, which is primarily targeted at low flux surveillance data has an effective flux scaling factor of 0.28.

The evidence for flux effects in low Cu steels is not agreed upon by the community. Several researchers have commented on the observed absence of flux effects in low Cu steels, particularly when considering the comparison of specific compositions of steels at low and

high flux but similar fluences [37]. Of most direct relevance is a previous study using ANNs found no effect of flux in the RADAMO database [22]. We note that the RADAMO database is generally composed of higher flux irradiations than the IVAR database (typically 0.2 to 8×10^{13} n/cm^{2}s^{-1}) it is possible that the flux effect will be less (or absent) in this region. An alternative explanation is the existence of additional hardening features that are thermally unstable at the irradiation temperature and therefore only produce significant populations at high flux when the formation rate becomes significant compared with the dissolution rate. At very high test reactor fluxes these unstable matrix defects provide a compensating increase in hardness that masks the delay in formation of matrix damage [40]. The influence of these defects has been discounted in the high flux data after careful examination of specific steel compositions [41].

5 Conclusions

This paper has developed models of irradiation embrittlement based on artificial neural network predictions from two different datasets. This has been done in order to examine the dependence of embrittlement on a range of variables and also to assess the performance of the model against various literature models. The neural network predictions perform with a similar level of uncertainty to literature-based models. It should be noted that many of the model plots present in the literature are based on predictions of data to which the model has already been fitted, rather than independent datasets, and therefore the quoted values of accuracy may be optimistic.

The dependence of the neural network predictions against various input parameters is largely in keeping with those expected from physically-based modelling. Where then do these non-mechanistic models sit within the requirements to predict accurately the degradation of a nuclear pressure vessel steel? As can be seen from Figures 7 and 10, the predictions from such

models may be associated with high levels of uncertainty particularly when extrapolating from the extent of an irradiation database. Their use in the prediction of end of life embrittlement for vessels may be limited therefore by this high uncertainty, given that even surveillance data are not representative of the true vessel wall conditions and require some extrapolation. They are however flexible and once setup do not require extensive work to refit as new data is added to the database. As reactors mature, the increased availability of surveillance data together with the older, higher total fluence vessels will change where in the dataspace the most important predictions arise and therefore we believe these sorts of networks provide a test of the reliability of existing models and any errors within the database. Where these mechanistic and non-mechanistic models agree, it is likely that the level of risk is low; where they are in conflict then this provides forewarning of a potential lack of understanding in the embrittlement predictions. This allows future irradiation damage programmes to be planned in a rational and informed basis.

Acknowledgements

JM, MEF and AC are grateful for funding from the Lloyd's Register Foundation, a charitable foundation helping to protect life and property by supporting engineering-related education, public engagement and the application of research.

References

[1] S.J. Zinkle, J.T. Busby. Structural materials for fission & fusion energy, Mater. Today. 12 (2009) 12–19.

[2] E.A. Marquis, J.M. Hyde, D.W. Saxey, S. Lozano-Perez, V. De Castro, D. Hudson, C.A. Williams, S. Humphry-Baker, D.W. Smith, Nuclear reactor materials at the atomic scale, Mater. Today. 12 (2009) 30–37.

[3] RSE-M Code. Rules for In-service Inspection of Nuclear Power Plant Components. AFCEN, Paris, 1997.

[4] E10 Committee, Practice for Design of Surveillance Programs for Light-Water Moderated Nuclear Power Reactor Vessels [Internet], West Conshohocken, PA: ASTM International, 2015 Jun. doi:10.1520/E0185-15E01

[5] JEAC4201-2004, Method of Surveillance Tests for Structural Materials of Nuclear Reactors, Japan Electric Association, Chiyoda-ku, Tokyo, Japan, December 2004.

[6] J.V. Pace, T.M. Rosseel, J.A. Wang, US NRC Embrittlement Data Base, 1999. Available: http://www.osti.gov/scitech/biblio/14353

[7] T. Allen, J. Busby, M. Meyer, D. Petti. Materials challenges for nuclear systems. Mater. Today. 13 (2010) 14–23.

[8] E. Altstadt, H.E. Ge, V. Kuksenko, M. Serrano, M. Houska, M. Lasan, M. Bruchhausen, J.-M. Lapetite, Y. Dai, Critical evaluation of the small punch test as a screening procedure for mechanical properties, J Nucl. Mater. 472 (2015) 186-195. doi:10.1016/j.jnucmat.2015.07.029

[9] E. Altstadt, E. Keim, H. Hein, M. Serrano, F. Bergner, H.-W.Viehrig, A. Ballesteros, R. Chaouadi, K. Wilford, FP7 Project LONGLIFE: Overview of results and implications, Nucl. Eng. Des. 278 (2014) 753–757.

[10] Reg. Guide 1.99. Radiation Embrittlement of Reactor Vessel Materials [Internet]. US Nuclear Regulatory Commission, May 1988. Report No.: Rev. 2. Available: http://www.nrc.gov/docs/ML0037/ML003740284.pdf

[11] C. Brillaud, F. Hedin, B. Houssin, A Comparison Between French Surveillance Program Results and Predictions of Irradiation Embrittlement. In: F. Garner, C. Henager, and N. Igata (Eds.), Influence of Radiation on Material Properties: 13th International Symposium (Part II). ASTM International, West Conshohocken, PA, 1987, pp. 420–447.

[12] E.D. Eason, G.R. Odette, R.K. Nanstad, T. Yamamoto. A physically-based correlation of irradiation-induced transition temperature shifts for RPV steels, J Nucl. Mater. 433 (2013) 240–254.

[13] N. Soneda, K. Dohi , A. Nomoto, K. Nishida, S. Ishino, Embrittlement Correlation Method for the Japanese Reactor Pressure Vessel Materials, Journal of ASTM International, 7 (2010) 1-20. doi.org/10.1520/JAI102127

[14] R. Ngayam-Happy, C.S. Becquart, C. Domain, First principle-based AKMC modelling of the formation and medium-term evolution of point defect and solute-rich clusters in a neutron irradiated complex Fe–CuMnNiSiP alloy representative of reactor pressure vessel steels, J Nucl.

Mater. 440 (2013) 143–152.

[15] P.B. Wells, T. Yamamoto, B. Miller, T. Milot, J. Cole, Y. Wu, G.R. Odette, Evolution of manganese–nickel–silicon-dominated phases in highly irradiated reactor pressure vessel steels, Acta Mater. 80 (2014) 205–219.

[16] A. Ballesteros, R. Ahlstrand, C. Bruynooghe, A. Chernobaeva, Y. Kevorkyan, D. Erak, D. Zurko, Irradiation temperature, flux and spectrum effects, Prog. Nuclear Energy. 53 (2011) 756–759.

[17] Report: IAEA-TECDOC-1441, Effects of nickel on irradiation embrittlement of light water reactor pressure vessel steels. International Atomic energy Agency, Vienna, Austria, June 2005.

[18] C.M. Bishop, Neural Networks for Pattern Recognition. First edition. Clarendon Press, Oxford, 1996.

[19] D.E. Rumelhart, G.E. Hinton, R.J. Williams. Learning representations by back-propagating errors, Nature Publishing Group, 323 (1986) 533–536.

[20] G.A. Cottrell, R. Kemp, H.K.D.H. Bhadeshia, G.R. Odette, T. Yamamoto. Neural network analysis of Charpy transition temperature of irradiated low-activation martensitic steels, J Nucl. Mater. 367–370 (2007) 603–609.

[21] R. Kemp, G.A. Cottrell, H.K.D.H. Bhadeshia, G.R. Odette, T. Yamamoto, H. Kishimoto, Neural-network analysis of irradiation hardening in low-activation steels. J Nucl. Mater. 348 (2006) 311–328.

[22] N. Castin, L. Malerba, R. Chaouadi, Prediction of radiation induced hardening of reactor pressure vessel steels using artificial neural networks, J. Nucl. Mater. 408 (2011) 30–39. doi:10.1016/j.jnucmat.2010.10.039.23.

[23] G.R. Odette, G.E. Lucas, D. Klingensmith, B.D. Wirth, D. Gragg, The Effects of Composition and Heat Treatment on Hardening and Embrittlement of Reactor Pressure Vessel Steels [Internet], NUREG/CR-6778, 2003 Available: http://www.nrc.gov/docs/ML0317/ML031700122.pdf

[24] L.H. Tsoukalas, R.E. Uhrig. Fuzzy and Neural Approaches in Engineering. First edition, New York, John Wiley & Sons, 1996.

[25] F. Rosenblatt, The perceptron: a probabilistic model for information storage and organization in the brain, Psychol. Rev. 65 (1958) 386–408. doi:10.1037/h0042519.

[26] MATLAB and Neural Network Toolbox Release 2012a, The MathWorks Inc., Natick, Massachusetts, United States.

[27] K. Hornik, M. Stinchcombe, H. White. Multilayer feedforward networks are universal approximators, Neural Networks, 2 (1989) 359-366.

[28] M.F. Møller, A Scaled Conjugate Gradient Algorithm for Fast Supervised Learning Supervised Learning, Neural Networks, 6 (1993) 525–533. doi:10.1016/S0893-6080(05)80056-5.

[29] D.J.C Mackay, Bayesian methods for Adaptive models, California Institute of technology, 1991.

[30] J. Hines, MATLAB supplement to Fuzzy and neural approaches in engineering. John Wiley & Sons, Inc. 1997.

[31] M.P. Perrone, When networks disagree: Ensemble methods for hybrid neural networks: in R.J.

Mammone (Ed.), Artificial Neural Networks for Speech and Vision, 1993, pp. 126-142.

[32] R. Chaouadi, R. Gérard, Copper precipitate hardening of irradiated RPV materials and implications on the superposition law and re-irradiation kinetics. J. Nucl. Mater. 345 (2005) 65–74.

[33] R.B. Jones, T.J. Williams, The Dependence of Radiation Hardening and Embrittlement on Irradiation Temperature, In: D.S. Gelles, R.K. Nanstad, A.S. Kumar, and A. Edward (Eds.), Effects of Radiation on Materials, 17th International Symposium, ASTM STP 1270, American Society for Testing and Materials, 1996, pp. 569-590.

[34] L. Debarberis, B. Acosta, A. Zeman, F. Sevini, A. Ballesteros, A. Kryukov, F. Gillemot, M. Brumovsky, Effect of irradiation temperature in PWR RPV materials and its inclusion in semi-mechanistic model. Scr. Mater. 53 (2005) 769–773.

[35] G.R. Odette, T. Yamamoto, D. Klingensmith, On the effect of dose rate on irradiation hardening of RPV steels. Philos. Mag. 85 (2005) 779–797.

[36] T.J. Williams, D. Ellis, C.A. English, J. Hyde, A model of irradiation damage in high nickel submerged arc welds. Int. J Press. Ves. Pip. 79 (2002) 649–660.

[37] P. Efsing, J. Rouden, P. Nilsson, Flux Effects on Radiation Induced Aging Behaviour of Low Alloy Steel Weld Material with High Nickel and Manganese Content, ASTM international: STP1572 (2014) doi:10.1520/STP157220130112

[38] R.E. Stoller, Non-steady-state conditions and in cascade clustering in radiation damage modeling, J Nucl. Mater. 244 (1997) 195–204.

[39] G.R. Odette, Modeling of microstructural evolution under irradiation, J Nucl. Mater.,85-86 (1979) 533–545.

[40] G.R. Odette, G.E. Lucas, Recent progress in understanding reactor pressure vessel steel embrittlement. Radiation Effects and Defects in Solids 144 (1998) 189–231.

[41] R. Chaouadi, R. Gérard, Confirmatory investigations on the flux effect and associated unstable matrix damage in RPV materials exposed to high neutron fluence. J Nucl. Mater. 437 (2013) 267–274.

Table and Figure captions

Table 1: Optimisation of function form of the fluence and flux parameters for training the artificial neural network

Table 2: Summary of average error and bias statistics from IVAR and NUREG training and validation datasets.

Figure 1: Plot comparing the fast neutron flux and fluence values used from the IVAR (green) and NUREG (blue) datasets. The solid and dashed lines show a comparative range of values expected at end-of-life for the inner wall of a US PWR and the typical surveillance capsule data assuming a lead-factor of four.

Figure 2: Plots showing the range of compositions within the IVAR dataset.

Figure 3: Moving average trendline showing the optimisation of neurons in the hidden layer based on minimisation of root mean square error (RMSE). Minimum test (red dotted line) and training error (blue dotted line) was first obtained with 11 neurons in the hidden layer.

Figure 4. Schematic representation of the ANN architecture used in this study: log-sigmoidal and linear transfer functions are used in the first and second layers.

Figure 5: Comparison of the measured values and the values predicted from the ANNs for both the IVAR and NUREG databases showing training data ((a) and (b)) and data reserved

for validation ((c) and (d)).

Figure 6: Variation in IVAR neural network estimated embrittlement shift as a function of temperature for (a) Cu contents of 0.04, and 0.5 wt. % and (b) Ni contents of 0.1 (low) and 1.5 wt.% (high) Other parameters (where not specified) are C_{Ni}=1.5, C_{Cu}=0.04, C_{Mn}=1.5, C_{Si}=0.2 and C_P=0.005 wt.%. Solid black lines denote linear fits to the data.

Figure 7: (a) Estimated transition temperature shift as a function of flux for low Cu, low and high Ni steels from NUREG database [6] (b) Efficiency of the neutrons at producing irradiation damage at higher fluxes normalised to a reference flux of 1.5×10^{11} n/cm^{2}s^{-1}. Values for other parameters were C_{Cu}=0.08, C_{Mn}=0.6, C_P=0.005, C_{Si}=0.2 wt%, the irradiation temperature was 290°C and the fluence was 8×10^{18} n/cm^2.

Figure 8: Variation in estimated embrittlement shift from the IVAR-based model [23] as a function of flux for (a) Ni contents of 0.1 (low) and 1.5 wt.% (high) (b) Mn contents of 0.1, and 1.5 wt. % and P contents of 0.002, and 0.05 wt. %. Other parameters were C_{Ni}=1.5, C_{Cu}=0.04, C_{Mn}=1.5, C_{Si}=0.2 and C_P=0.005 wt.%. Data points are fitted using spline interpolation.

Figure 9: Embrittlement shift variation expressed as a function of interactions of chemical composition for (a) Ni and Cu (b) Ni and Mn (c) Ni and Si (d) Ni and P. Other parameters not given were C_{Ni}=1.5, C_{Cu}=0.04, C_{Mn}=1.5, C_{Si}=0.2 and C_P=0.005 wt.%.

Figure 10: Prediction curves for CM16 and CM17 showing IVAR data (purple squares), EONY model prediction (red curve) [12] and ANN prediction bounds (black lines) showing

central prediction and plus and minus one standard deviation.

Figure 11: Plot of the b/a ratio as calculated from linear fits to the ANN model predictions and compared with the literature Jones and Williams (J&W) value for carbon-manganese steels [33]. Values of parameters not given in the figure are: C_{Ni}=1.5, C_{Cu}=0.04, C_{Mn}=1.5, C_{Si}=0.2 and C_P=0.005 wt.%. High and low fluence values are 1×10^{19} and 3×10^{19} n/cm^2 and a flux of 3×10^{11} n/cm^{2}s^{-1}.

Figure 12: Plot showing the variation of the flux scaling parameter p across the IVAR flux range (p=0 would be no flux effect) for three different temperatures. Values of parameters are: C_{Ni}=1.5, C_{Cu}=0.04, C_{Mn}=1.5, C_{Si}=0.2 and C_P=0.005 wt.%. The value of fluence is 3×10^{19} n/cm^2.

Tables

Table 1: Optimisation of function form of the fluence and flux parameters for training the artificial neural network

Functional form	$RMSE_{training}$
F(fluence, flux)	24.75
F(fluence$^{1/2}$, flux$^{1/2}$)	21.75
F(log(fluence), log(flux))	26.59

Table 2: Summary of average error and bias statistics from IVAR and NUREG training and validation datasets.

Database	***Avg. Error, MPa***	***Avg. Bias, MPa***
IVAR (training)	17.9	0.23
IVAR (validation)	16.1	11.5
NUREG (training)	22.6	0.96
NUREG (validation)	30.7	5.9

Figures

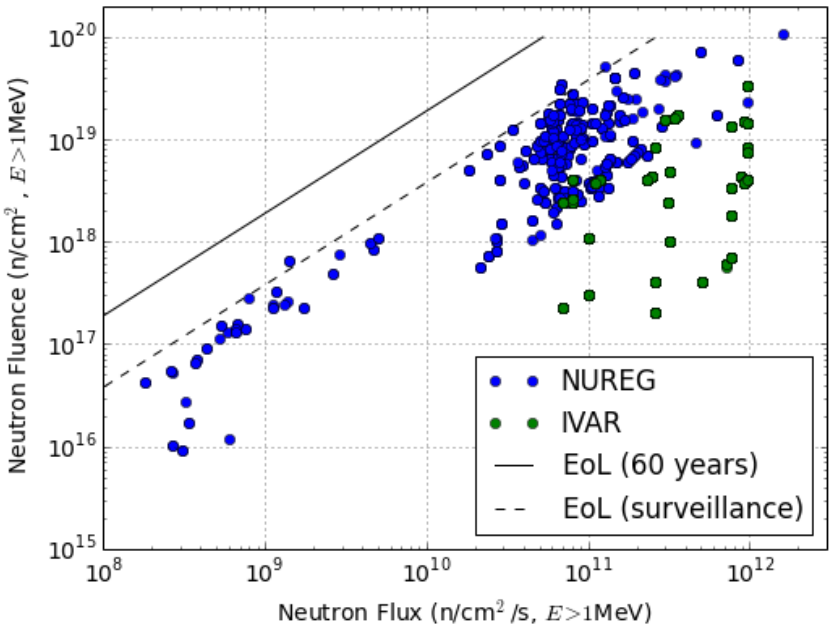

Figure 1: Plot comparing the fast neutron flux and fluence values used from the IVAR (green) and NUREG (blue) datasets. The solid and dashed lines show a comparative range of values expected at end-of-life for the inner wall of a US PWR and the typical surveillance capsule data assuming a lead-factor of four.

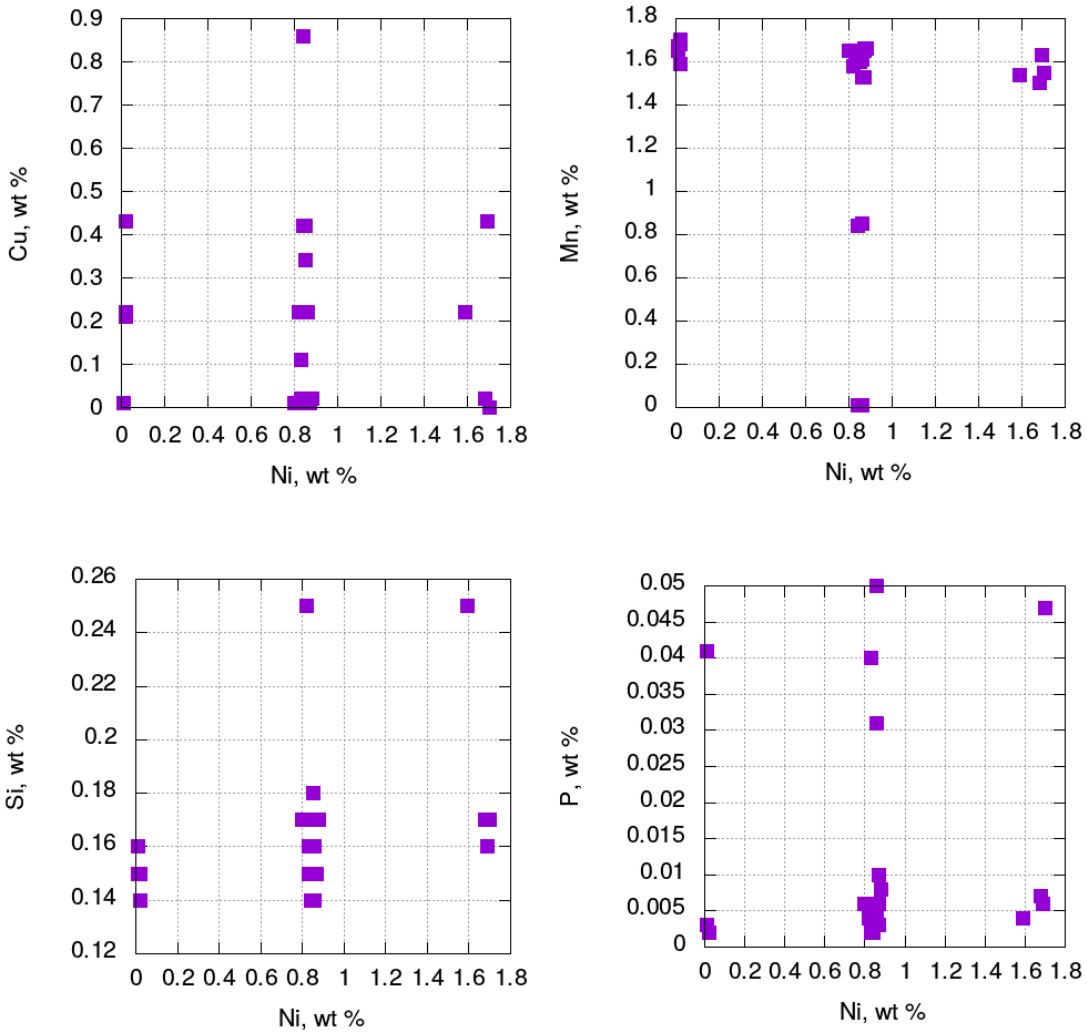

Figure 2: Plots showing the range of compositions within the IVAR dataset.

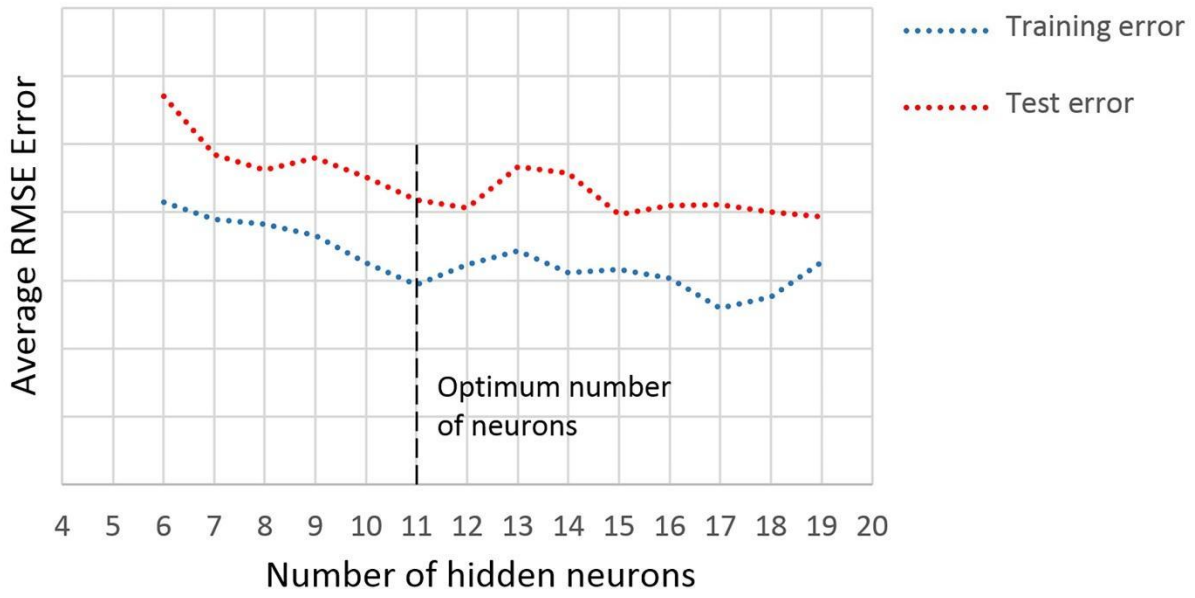

Figure 3: Moving average trendline showing the optimisation of neurons in the hidden layer based on minimisation of root mean square error (RMSE). Minimum test (red dotted line) and training error (blue dotted line) was first obtained with 11 neurons in the hidden layer.

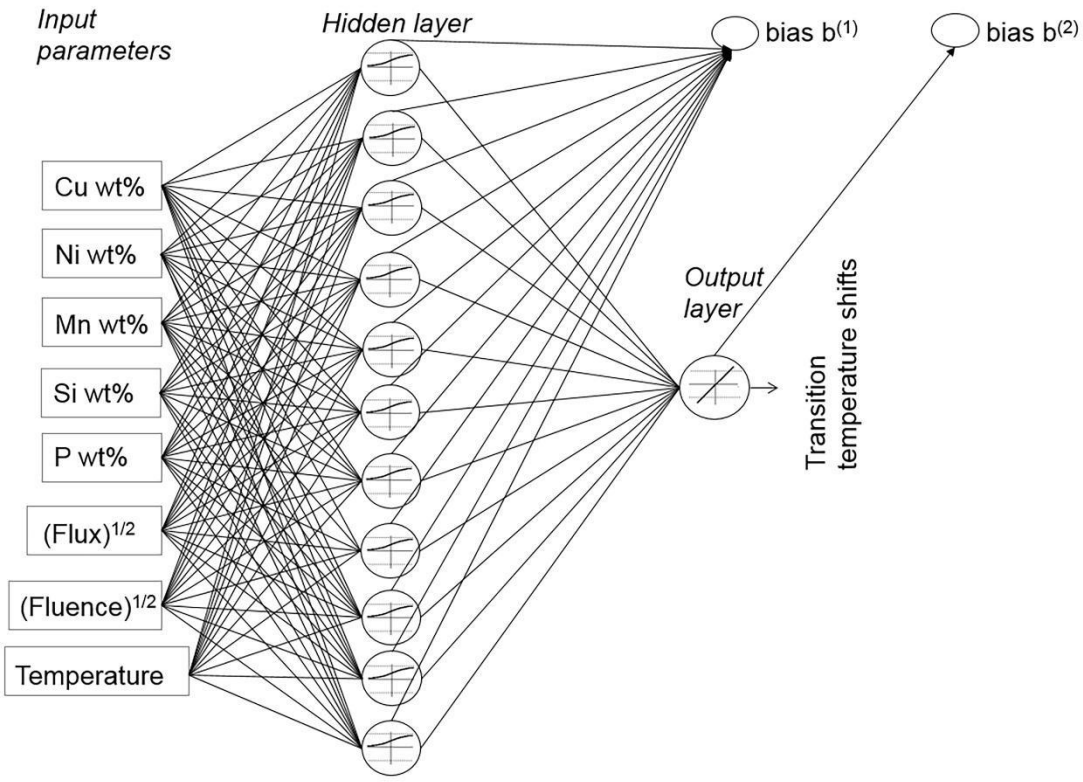

Figure 4. Schematic representation of the ANN architecture used in this study: log-sigmoidal and linear transfer functions are used in the first and second layers.

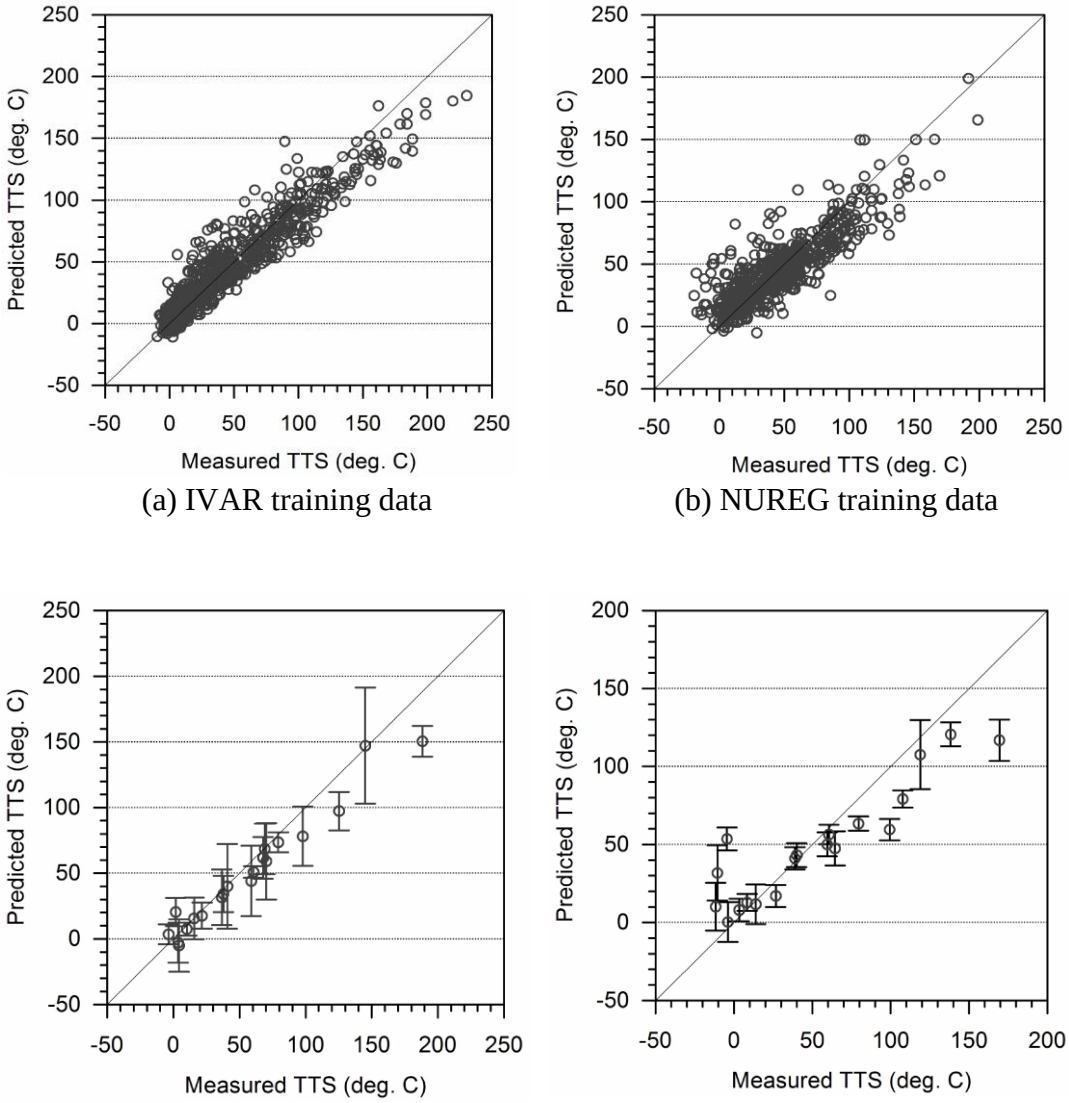

(a) IVAR training data

(b) NUREG training data

(c) IVAR test data

(d) NUREG test data

Figure 5: Comparison of the measured values and the values predicted from the ANNs for both the IVAR and NUREG databases showing training data ((a) and (b)) and data reserved for validation ((c) and (d)).

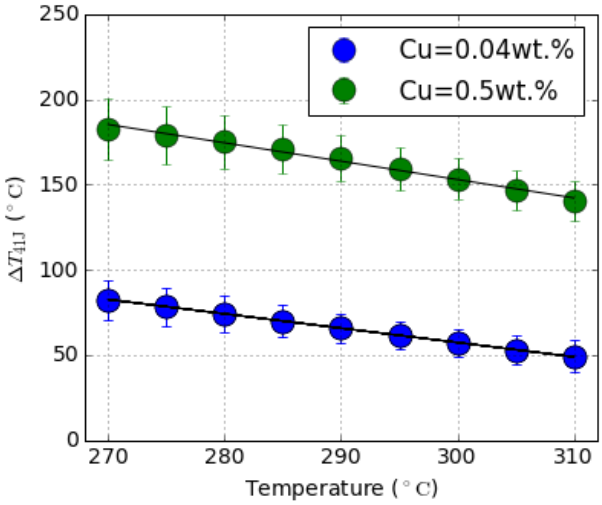

(a)

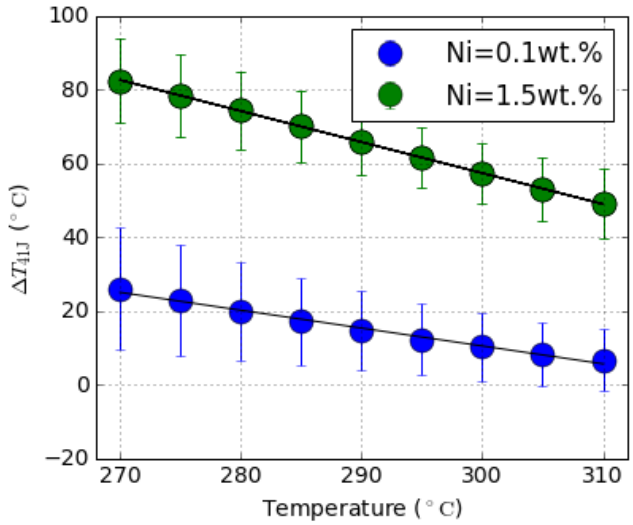

(b)

Figure 6: Variation in IVAR neural network estimated embrittlement shift as a function of temperature for (a) Cu contents of 0.04, and 0.5 wt. % and (b) Ni contents of 0.1 (low) and 1.5 wt.% (high) Other parameters (where not specified) are C_{Ni}=1.5, C_{Cu}=0.04, C_{Mn}=1.5, C_{Si}=0.2 and C_P=0.005 wt.%. Solid black lines denote linear fits to the data.

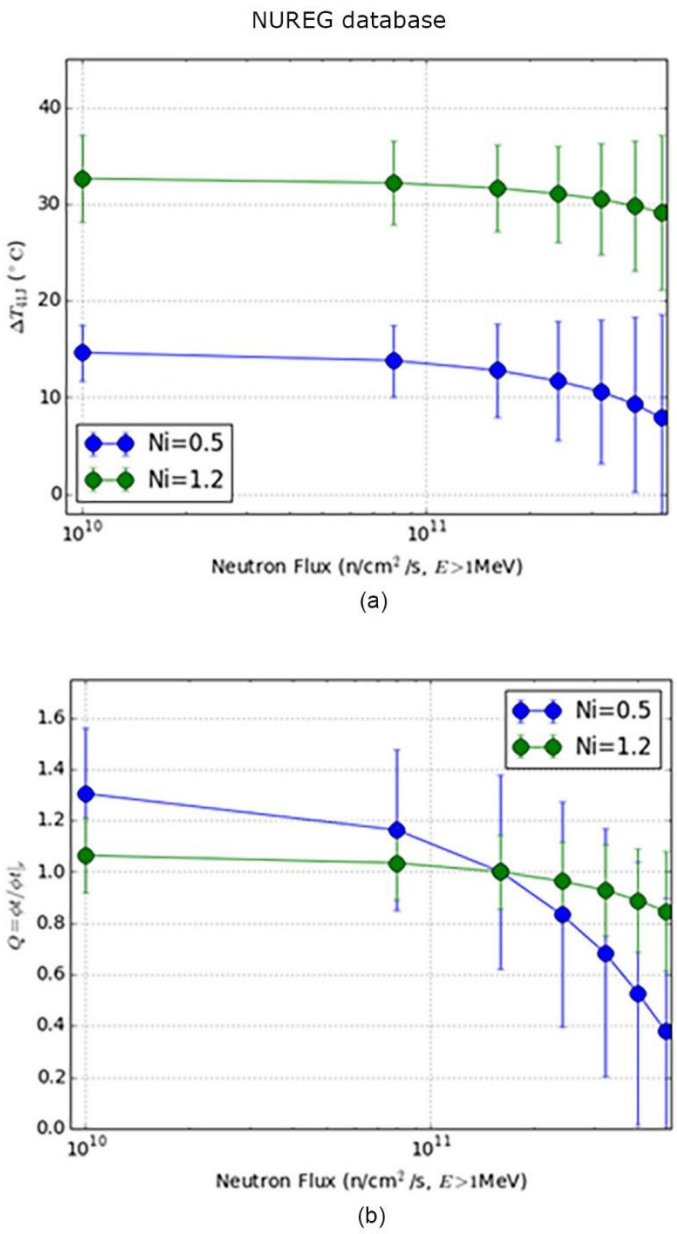

Figure 7: (a) Estimated transition temperature shift as a function of flux for low Cu, low and high Ni steels from NUREG database [6] (b) Efficiency of the neutrons at producing irradiation damage at higher fluxes normalised to a reference flux of 1.5×10^{11} n/cm^{2}s^{-1}. Values for other parameters were C_{Cu}=0.08, C_{Mn}=0.6, C_P=0.005, C_{Si}=0.2 wt%, the irradiation temperature was 290°C and the fluence was 8×10^{18} n/cm^2.

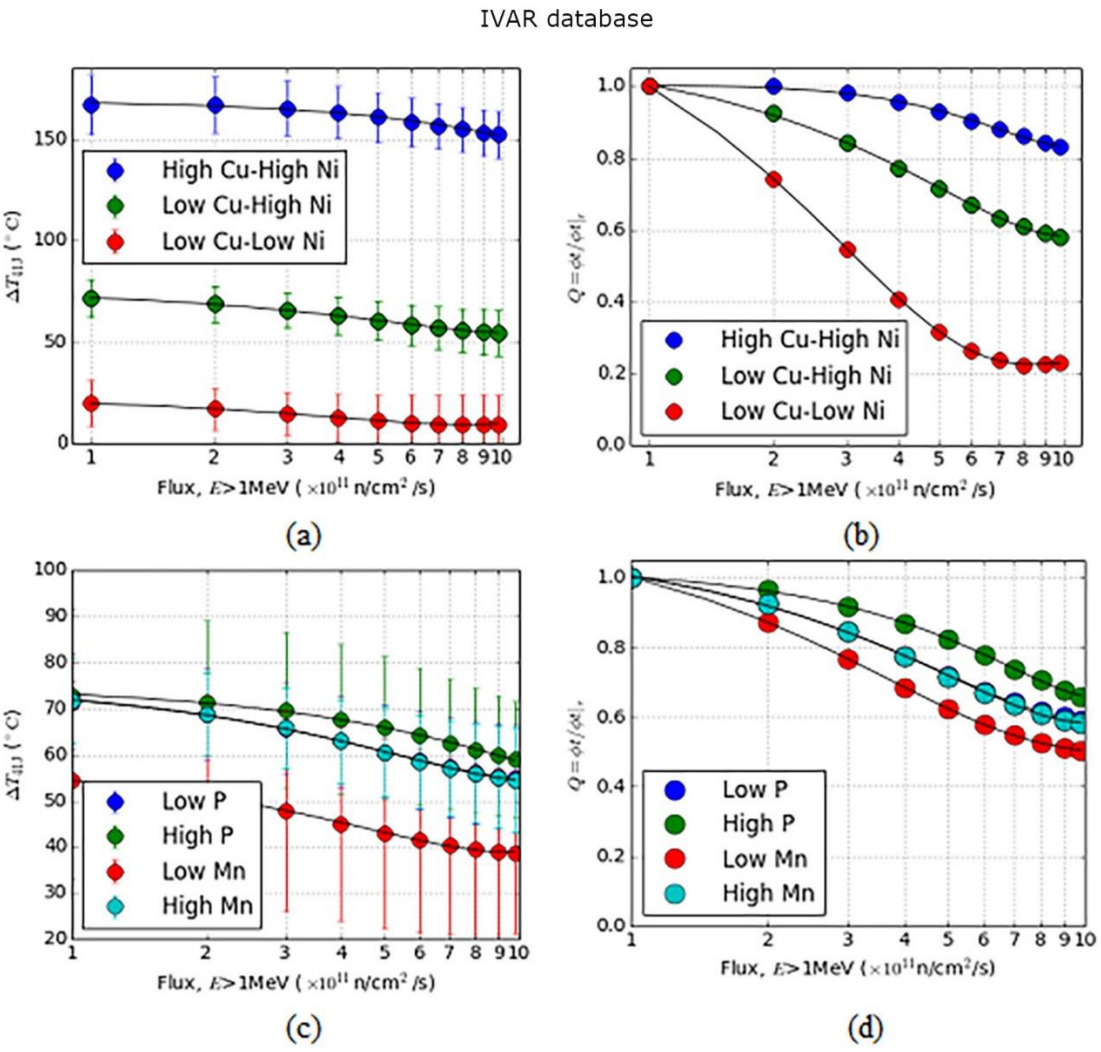

Figure 8: Variation in estimated embrittlement shift from the IVAR-based model [23] as a function of flux for (a) Ni contents of 0.1 (low) and 1.5 wt.% (high) (b) Mn contents of 0.1, and 1.5 wt. % and P contents of 0.002, and 0.05 wt. %. Other parameters were C_{Ni}=1.5, C_{Cu}=0.04, C_{Mn}=1.5, C_{Si}=0.2 and C_P=0.005 wt.%. Data points are fitted using spline interpolation.

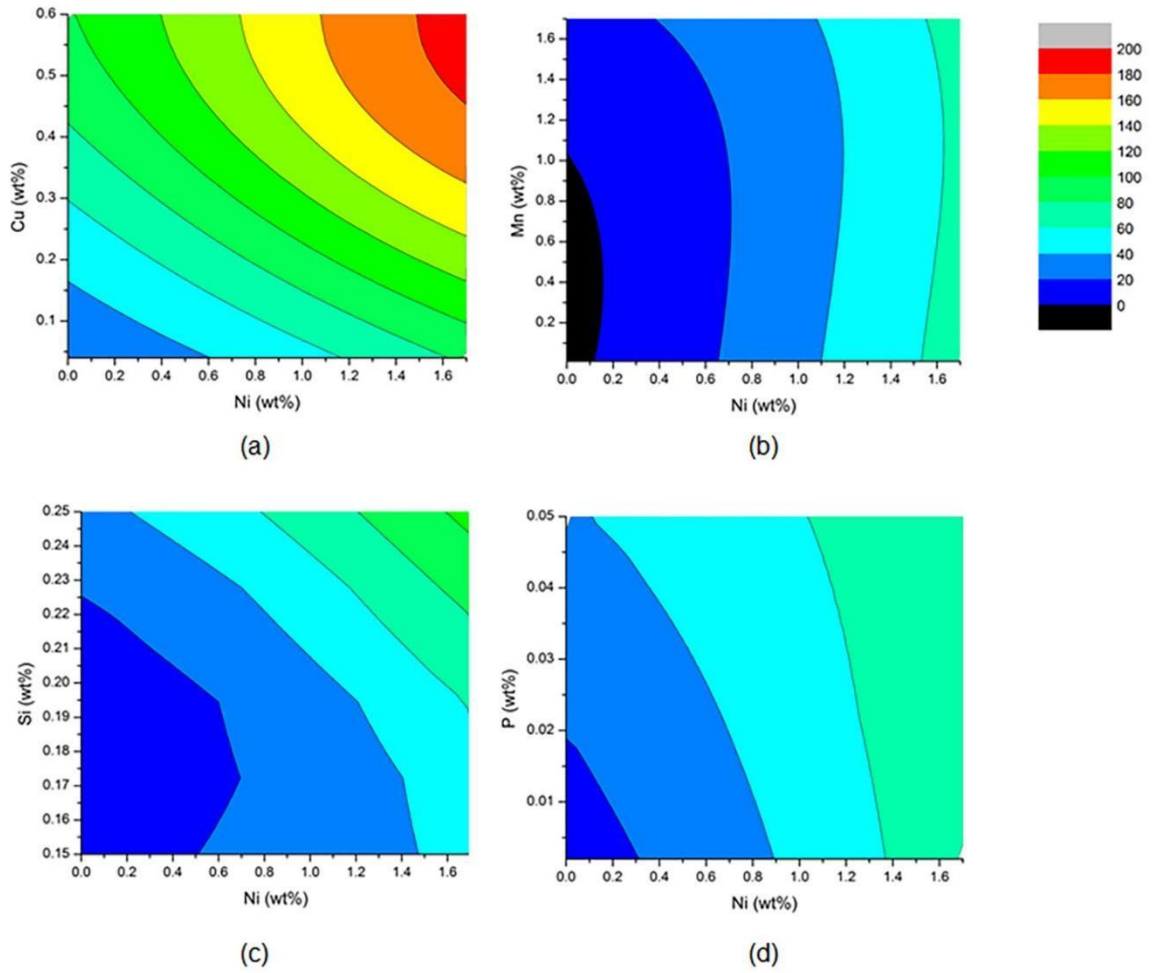

Figure 9: Embrittlement shift variation expressed as a function of interactions of chemical composition for (a) Ni and Cu (b) Ni and Mn (c) Ni and Si (d) Ni and P. Other parameters not given were C_{Ni}=1.5, C_{Cu}=0.04, C_{Mn}=1.5, C_{Si}=0.2 and C_{P}=0.005 wt.%.

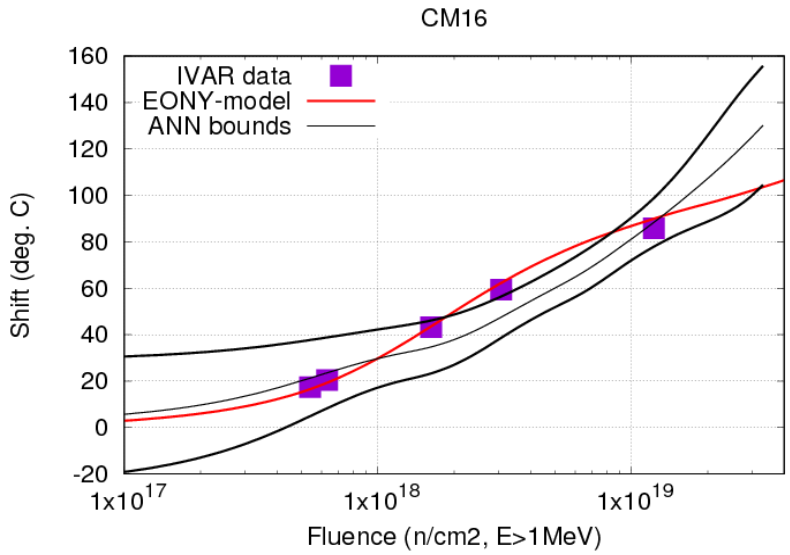

(a)

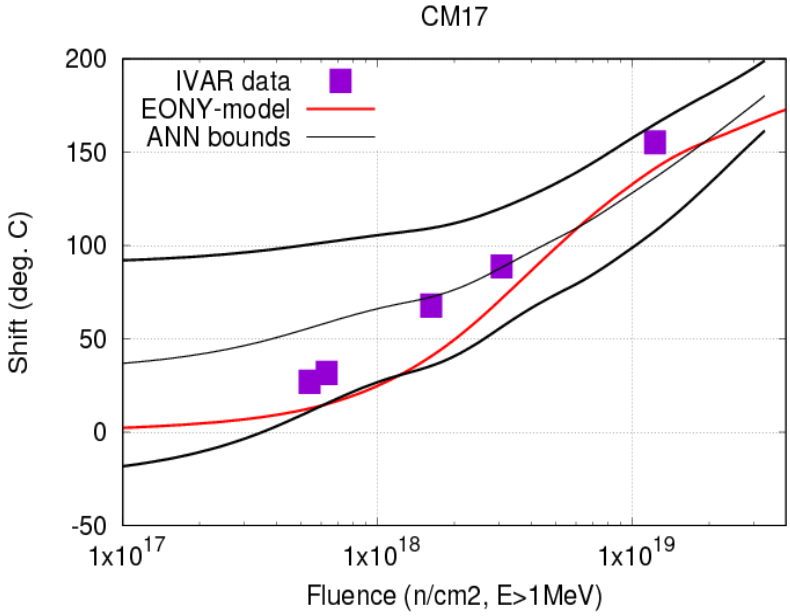

(b)

Figure 10: Prediction curves for CM16 and CM17 showing IVAR data (purple squares), EONY model prediction [12] (red curve) and ANN prediction bounds (black lines) showing central prediction and plus and minus one standard deviation.

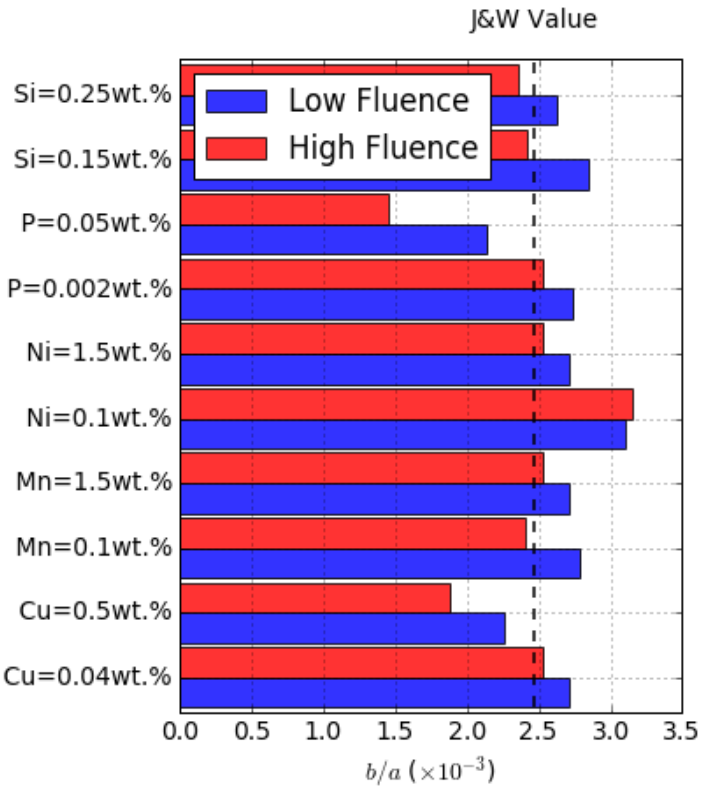

Figure 11: Plot of the *b*/*a* ratio as calculated from linear fits to the ANN model predictions and compared with the literature Jones and Williams (J&W) value for carbon-manganese steels [33]. Values of parameters not given in the figure are: C_{Ni}=1.5, C_{Cu}=0.04, C_{Mn}=1.5, C_{Si}=0.2 and C_P=0.005 wt.%. High and low fluence values are 1×10^{19} and 3×10^{19} n/cm^2 and a flux of 3×10^{11} n/cm^{2}s^{-1}.

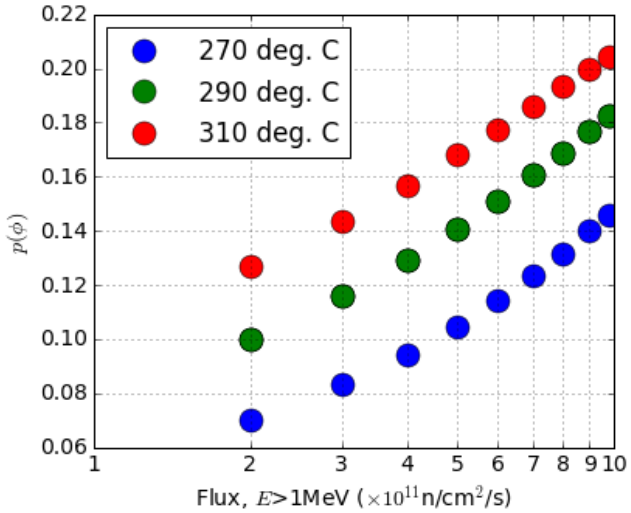

Figure 12: Plot showing the variation of the flux scaling parameter *p* across the IVAR flux range (*p*=0 would be no flux effect) for three different temperatures. Values of parameters are: C_{Ni}=1.5, C_{Cu}=0.04, C_{Mn}=1.5, C_{Si}=0.2 and C_{P}=0.005 wt.%. The value of fluence is 3×10^{19} n/cm^2.